The structure and evolution of a sigmoidal active region

S. E. Gibson[1] and L. Fletcher[2]

G. Del Zanna[3], C. D. Pike[4], H. E. Mason[3], C. H. Mandrini[5], P. Démoulin[6], H. Gilbert[1], J. Burkepile[1], T. Holzer[1], D. Alexander[7], Y. Liu[8], N. Nitta[7], J. Qiu[9], B. Schmieder[6], B. J. Thompson[10]

ABSTRACT

Solar coronal sigmoidal active regions have been shown to be precursors to some coronal mass ejections (CMEs). Sigmoids, or "S"-shaped structures, may be indicators of twisted or helical magnetic structures, having an increased likelihood of eruption. We present here an analysis of a sigmoidal region's 3-d structure and how it evolves in relation to its eruptive dynamics. We use data taken during a recent study of a sigmoidal active region passing across the solar disk (an element of the third "Whole Sun Month" campaign). While S-shaped structures are generally observed in soft X-ray (SXR) emission, the observations we present demonstrate their visibility at a range of wavelengths including those showing an associated sigmoidal filament. We examine the relationship between the S-shaped structures seen in SXR and those seen in cooler lines in order to probe the sigmoidal region's 3-d density and temperature structure. We also consider magnetic field observations and extrapolations in relation to these coronal structures.

---

[1]HAO/NCAR, p.o. box 3000, Boulder, CO, 80307, U.S.A.

[2]Dept. of Physics and Astron., Univ. of Glasgow, Glasgow G12 8QQ, U.K.

[3]DAMTP, Univ. of Cambridge, Silver St., Cambridge, CB3 9EW, U.K.

[4]Rutherford Appleton Laboratory, Chilton, Didcot, Oxfordshire, OX11 0QX, U.K.

[5]Instituto de Astronomía y Física del Espacio, IAFE, CC. 67 Suc. 28, 1428 Buenos Aires, Argentina.

[6]Observatoire de Paris, section Meudon, DASOP, URA 2080 (CNRS), F-92195 Meudon Principal Cedex, France.

[7]Lockheed Martin Solar and Astrophysics Lab, Org L9-41/B252, 3251 Hanover St, Palo Alto, CA 94304.

[8]HEPL/CSSA, Stanford University, Stanford, CA 944305-4085

[9]Big Bear Solar Observatory, New Jersey Institute of Technology, 40386 North Shore Lane, Big Bear City, CA 92314-9672.

[10]NASA/GSFC, Code 682, Greenbelt, MD, 20771.

We present an interpretation of the disk passage of the sigmoidal region, in terms of a twisted magnetic flux rope that emerges into and equilibrates with overlying coronal magnetic field structures, which explains many of the key observed aspects of the region's structure and evolution. In particular, the evolving flux rope interpretation provides insight into why and how the region moves between active and quiescent phases, how the region's sigmoidicity is maintained during its evolution, and under what circumstances sigmoidal structures are apparent at a range of wavelengths.

Subject headings: corona—Sun, coronal mass ejections—Sun, flares—Sun, sigmoids—Sun

1. Introduction

Coronal mass ejections (CMEs) are fascinating demonstrations of the complexity and power of magnetohydrodynamic processes at the Sun. "Sigmoids", the name given to S-shaped (or inverse-S-shaped) coronal active regions as seen in soft X-ray emission, have been shown to be precursors to CMEs (Manoharan et al. (1996); Hudson et al. (1998); Rust and Kumar (1996); Sterling and Hudson (1998); Pevtsov and Canfield (1999)) and statistically more likely to erupt (Canfield et al. (1999)). Interestingly, although these regions can be sites of greater than usual activity, the overall S or inverse-S shape can survive for days or weeks. Thus the basic configuration of the sigmoidal active region is almost paradoxically stable.

Many of the analyses to date have concentrated on X-ray observations of sigmoids, often in relation to magnetic field observations, because X-ray is the frequency regime where sigmoids are most commonly monitored (Hudson et al. (1998); Sterling and Hudson (1998); Canfield et al. (1999); López Fuentes et al. (2000); Moore et al. (2001)). H-α observations of sigmoidal filaments have also been studied (Rust and Kumar (1996); Pevtsov et al. (1996); Lites and Low (1997); Gibson and Low (2000); Pevtsov (2002)). However, these two extremes show only the hottest and coldest material associated with the sigmoidal region. A multi-wavelength study is required to probe the entire structure, and to consider how the sigmoid plasma relates to its underlying magnetic field. A few such detailed analyses of specific sigmoid-related flares and CMEs have recently been done (Sterling et al. (2000); Zarro et al (1999); Wang et al. (2001); Aurass et al. (2001)), as well as surveys of the general characteristics of sigmoids at a range of temperatures (Gibson et al. (1999b); Glover et al. (2001)).

In August, 1999, a multi-wavelength analysis of a sigmoidal active region was run, as part of the third Whole Sun Month (WSM3) campaign. Observations included data from the Solar and Heliospheric Observatory (SOHO), Transition Region and Coronal Explorer (TRACE), Yohkoh, Big Bear Solar Observatory (BBSO), Meudon Observatory, and Mauna Loa Solar Observatory (MLSO) telescopes. The Whole Sun Month campaigns have provided excellent opportunities for observers and modelers to work together to describe the 3-d morphology, plasma properties, and magnetic field of the global corona, and to connect these structurally to *in situ* observations (Biesecker et al. (1999); Galvin and Kohl (1999); Gibson et al. (1999a)). The WSM3 campaign studied the global corona during the ascending phase of the solar cycle, and consisted of several Joint Observing Programs (JOPs), among them the sigmoidal active region study (SOHO/TRACE JOP 106). This JOP provided the first opportunity to study a sigmoidal region in depth and at multiple wavelengths as it crossed the solar disk. Thus we were able to analyze its structure from multiple lines-of-sight and temperature regimes, and study how its evolution related to dynamic events on the Sun during its passage.

Section 2 of this paper will describe observations of how the sigmoidal region evolved and exhibited coronal activity as it crossed the disk. Details of the activity in the region are specified in the timeline of Table 1. Section 3 will present analyses of the physical structure (magnetic field, density, temperature, and velocity) of the region. The large volume of detailed data obtained in the campaign covers nearly two weeks and a wide range of frequencies. Therefore, in order to make sense of what otherwise might be an overwhelming amount of observational information, we summarize some questions raised by the observations at the end of each of these sections. Moreover, in Section 4 we will present a possible theoretical interpretation of the observed sigmoid structure and evolution, in terms of a magnetic flux rope emerging into and equilibrating with the coronal environment. In particular, we will consider the observed behavior of the region, where first the sigmoidal region is active, with multiple flares and associated eruptions, then it moves on to a relatively quiescent stage, and then destabilizes amid emerging magnetic flux and further X-ray activity and eruptions. Such behavior is consistent with a flux rope that emerges, interacts with its external environment until it reaches a metastable equilibrium, is destabilized by new emerging magnetic flux and other changes in its environment, and again goes through the process of equilibrating via flaring and eruptions and possibly a partial ejection of the rope itself. In Section 5 we present our conclusions.

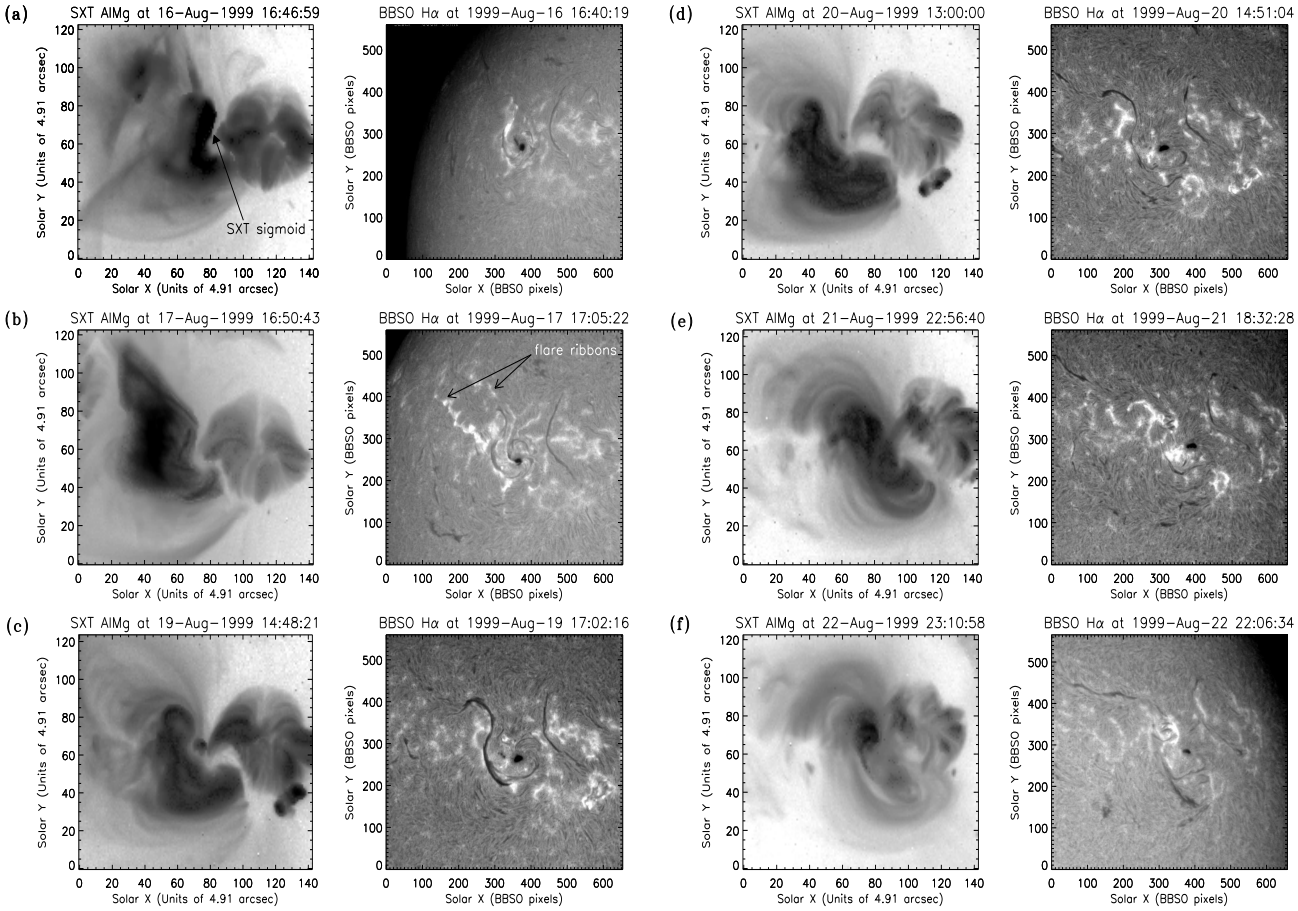

Fig. 1.— Yohkoh/SXT X-ray (left columns - inverted color table) and BBSO H-α (right columns) observations of sigmoidal active region 8668, August 16, 17, 19, 20, 21, and 22, 1999.

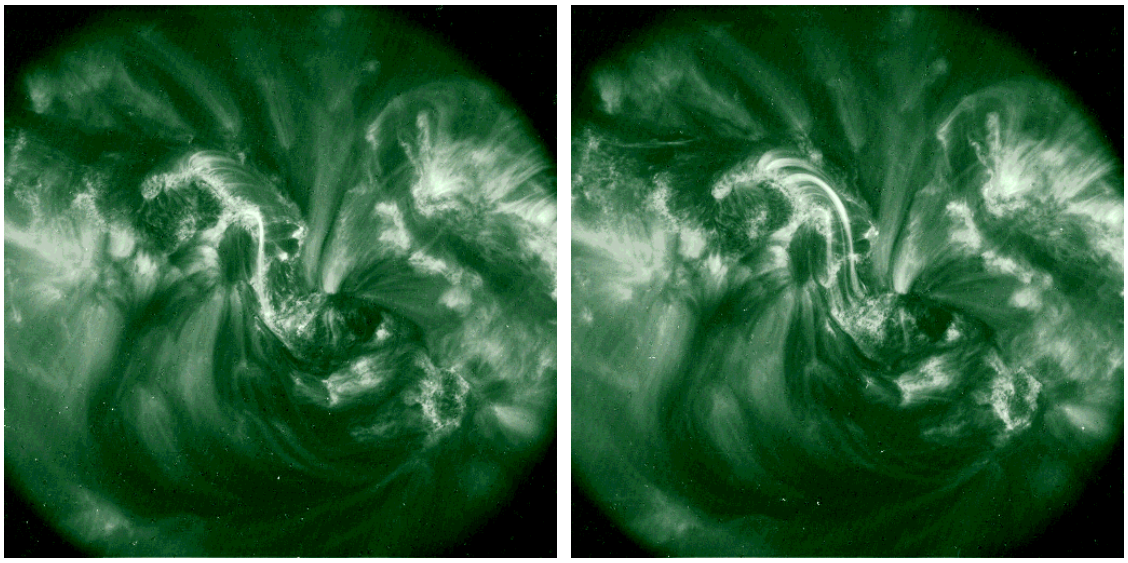

Fig. 2.— TRACE 195 Angstrom emission of sub-sigmoid brightening on August 21, 1999 at a) 18:26 UT (left) and b) 18:51 UT (right). Note that these images are logarithmically scaled.

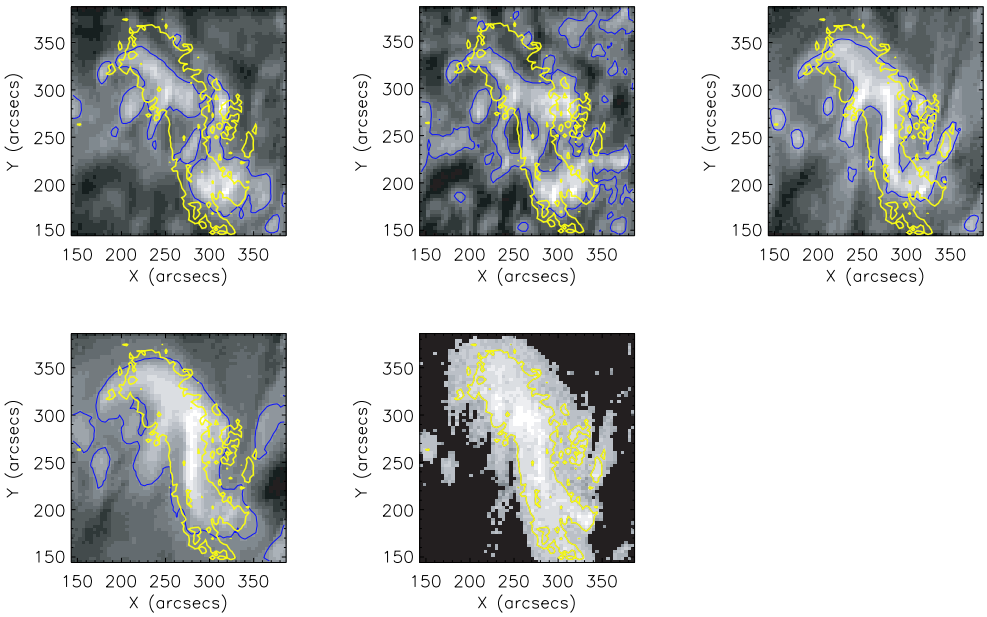

Fig. 3.— SOHO/CDS emission of sub-sigmoid brightening on August 21, 1999, at 18:21 UT, in (clockwise from upper left) HeI, OV, MgX, FeXIX, and SiXII. Contours from each line are overlaid in blue, the additional thick yellow contours overlaid are from FeXIX.

2. Evolution of the sigmoidal active region

2.1. Summary of activity associated with the sigmoidal region

Extensive activity was associated with our sigmoidal region during its passage across the solar disk. Identified as NOAA AR8668, it appeared at the limb of the northeast (NE) quadrant approximately on August 12, 1999, had a large CME associated with it on August 14, and became identifiable as an inverse-S oriented sigmoid on August 16 using X-ray images taken by the Yohkoh/Soft X-ray Telescope (SXT) satellite. The WSM3 streamer study (SOHO/TRACE JOP 76) immediately targeted a neighboring streamer in the NE as a good candidate for eruption, and indeed, on August 17 the streamer with its associated polar crown filament blew out in a coronal mass ejection. This CME was accompanied by flaring in AR8668 (we will discuss the relationship between the CME and AR8668 in more detail below). These flares were part of a series of B and C class flares observed in AR8668 between August 16-17 (*Canfield et al., paper in preparation*). An inverse-S-shaped filament, clearly visible in H-α and more or less aligned with the X-ray sigmoid, formed in stages along the neutral line starting on August 16 (Figures 1 a, 1 b), was at its largest and most continuously apparent on August 18 and most of August 19 (Figure 1 c), underwent disappearance as new flux emerged near its midpoint between August 20-21 (Figures 1 d and 1 e), and then may have partially re-established itself along portions of the significantly altered neutral line between August 22-24 (Figure 1 f). On August 21 a small flare-like brightening event showed sigmoidal structure at a range of wavelengths (Figures 2, 3) (note that throughout this paper, we will only refer to a flare if it is GOES classified – otherwise we will refer to brightenings or flare-like brightenings). Finally, a jet that may have been associated with this sigmoidal region occurred on August 26, when AR8668 was at the west limb (*Ko et al., paper in preparation*).

Throughout the sigmoidal region's disk passage, X-ray loops continued to reform into identifiable inverse-S shapes between events until projection effects made such identification impossible. Likewise the sigmoidal filament appeared and disappeared in H-α, lying along the underlying inverse-S-shaped neutral line (although after the new magnetic flux emerged, the neutral line's inverse-S shape was essentially disrupted). One of the questions we wished to address with our multi-wavelength study was to what extent sigmoidal structures became visible in temperatures other than the very hot (3-5 million Kelvin) X-ray loops or the cold (5-10,000 Kelvin) H-α filament. A preliminary survey of SOHO/Coronal Diagnostics Spectrometer (CDS) (Harrison et al. (1995)) observations of regions designated sigmoidal by X-ray observations (Canfield et al. (1999)) found evidence for S-shaped structures at a range of temperatures (20,000 - 1 million Kelvin; HeI - SiXII) (Gibson et al. (1999b)). However, observations of the disk passage of AR8668 demonstrated that our sigmoid was not

obvious at most temperatures, with the notable exception of the small inverse-S brightening of August 21 which was visible in emission at a range of temperatures (Figures 2, 3). This multi-wavelength brightening will be discussed further in Section 3.

2.2. Details of sigmoidal region evolution

In order to better interpret the observations, we will now present details of the sigmoidal region's evolution for four key time periods: 1) the "active" period of multiple flares and the NE CME (August 16-17), 2) the relatively quiescent period of the "stable" sigmoidal filament (August 18-19), 3) the period of filament disintegration and further CME/X-ray activity (August 20-21), and finally 4) the observations of what remained of the sigmoidal region as it approached the west limb (August 22-26). A timeline of observations can be found in Table 1.

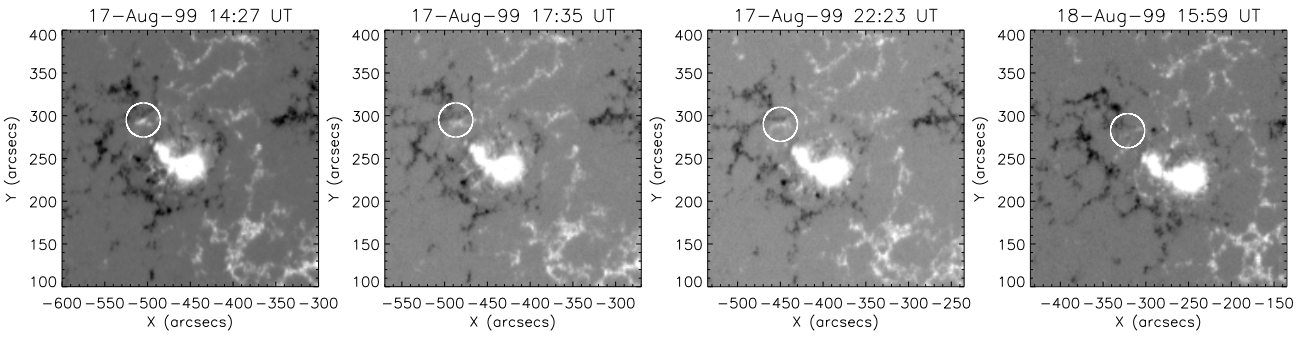

Fig. 4.— August 17-18, 1999: MDI observations of magnetic field - note the small white (positive) field to the northeast of the main white sunspot. Over the course of the first three images (August 17: 14:27 UT, 17:35 UT, 22:23 UT) it disappears, with no trace remaining the following day (right-hand image, August 18: 15:59 UT).

August 16th and 17th, 1999: flares and filament formation. Prior to and early on August 16th, to the extent establishable using near-limb observations, some filament material was intermittently visible in both the northern and the southern portions of an inverse-S-shaped filament channel, although often not at the same time. The appearance of the southern part of the inverse-S-shaped filament on the afternoon of August 16th was accompanied by flaring (GOES C-class) along the filament channel (Figure 1 a) (note that the large cusp seen in X-rays in the southern part of the sigmoid on August 16th is associated with earlier activity, possibly the CME of August 14th). Meanwhile, filament material in the northern portion of the inverse-S-shaped filament channel was intermittently visible, and appeared to erupt (or at least disappear) at least once (see Table 1). During this activity the southern portion of the filament did not greatly change. On August 17th, the northern extension of the filament appeared to stabilize after an initial C-class flare and during a subsequent C-class flare (which led to the small cusp in the northern part of the X-ray sigmoid visible in Figure 1 b). Interestingly, SOHO/Michelson Doppler Imager (MDI) observed a magnetic flux cancellation near the midpoint between the northern and southern portions of the inverse-S-shaped filament, just as the northern portion of the filament was apparently stabilizing (Figure 4).

The activity on August 17th was not limited to the immediate vicinity of our sigmoidal region. The first C-class flare occurred along the S-shaped neutral line, and was quickly followed by 1) a dimming as observed by SOHO/Extreme ultraviolet Imaging Telescope (EIT) extending up to the northeast of AR8668 (see Thompson et al. (1999) for a discussion of SOHO/EIT dimmings and their relation to CMEs), 2) a streamer deflection on the NE limb observed by SOHO/EIT and the appearance of a CME in SOHO/Large Angle and Spectrometric Coronagraph (LASCO) C2 white light observations, 3) a second GOES C-class flare in AR8668 accompanied by a Yohkoh/SXT cusp and a two-ribbon flare visible in H-α and later by post-flare loops visible in SOHO/EIT and Yohkoh/SXT, and 4) the launching of a polar crown filament to the north of AR8668. In the midst of the later part of this activity the northern portion of the sigmoidal filament became steadily more visible, as indicated by BBSO H-α observations beginning just after the second C-class flare. Note that H-α data (when it was available), indicated that the southern portion of the filament remained visible throughout the activity of August 17th. (See Table 1 for specifics on the times of these observations, and *http* : *//hao.ucar.edu/ sgibson/SIGMOID/* for EIT movies illustrating the spatial and temporal connections between AR8668 and the CME-related activity.)

August 18th - 19th: growth of the filament. After the flare of August 16th for the southern portion, and the flares on August 17th for the northern portion, each portion had a temporarily quiescent phase, so that for much of August 18th and 19th a filament was visible along the entire inverse-S-shaped neutral line (Figure 1 c). Incomplete H-α data

coverage necessarily qualifies this conclusion (see Table 1 for specific times of coverage), however, continuous SOHO/EIT and SOHO/LASCO data for August 18-19 do not indicate any obvious white light CMEs or large flares associated with the region, and also no new Yohkoh/SXT cusps appeared in AR8668 in this time period. There was some brightening in the southern part of the sigmoid seen by SOHO/EIT and Yohkoh/SXT, and this was accompanied by some evolution of the southern filament as observed in H-α, so that the southern portion of the filament appeared fairly thin for parts of August 18th. By August 19th, however, the southern portion had grown to its greatest apparent width, and a full, clear sigmoid outlining the entire inverse-S was visible in H-α observations (see Figure 1 c). We also note that while the H-α sigmoidal filament had its most obvious inverse-S shape during this time, the X-ray sigmoid was less apparent, with mostly the fat southern loops evident (Figure 1 c).

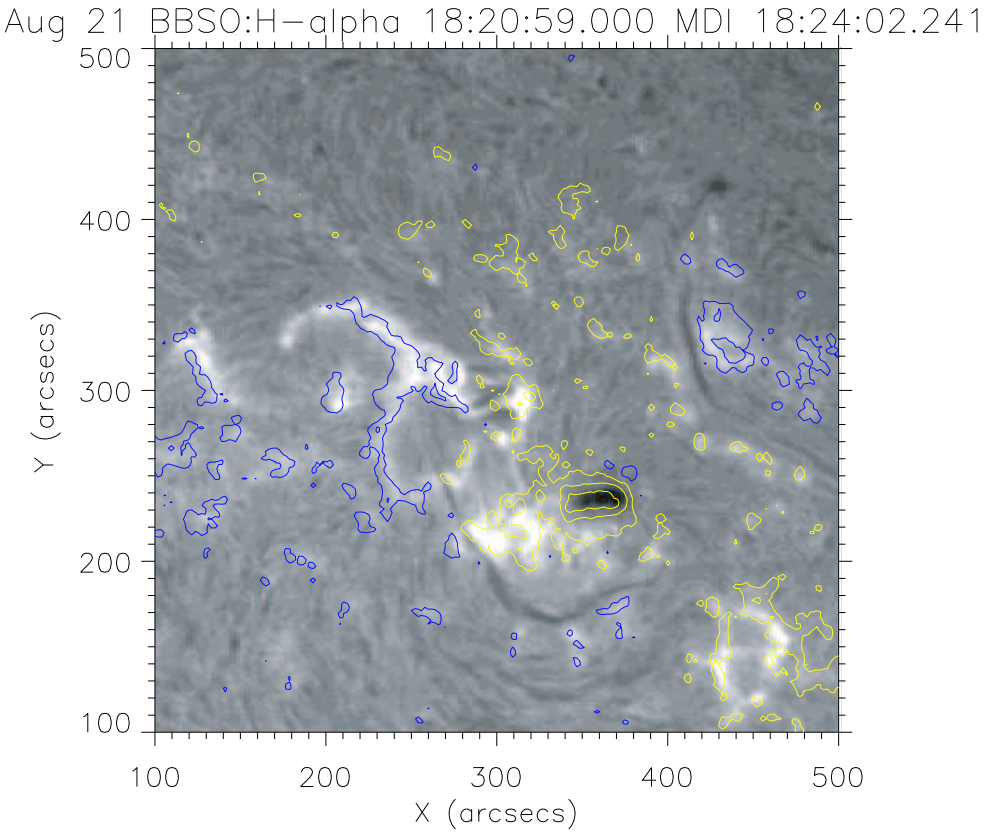

Fig. 5.— August 21, 1999: BBSO H-α observations, with contours of MDI observations of magnetic field overlaid (blue: negative, yellow: positive). Note the emerging flux region (EFR) which appears as a small magnetic bipole in the middle of the figure, with an arched filament system (AFS) seen in H-α visible as dark horizontal lines connecting the ends of the magnetic bipole.

August 20th - 21st: filament disintegration and eruption. Very late on August 19th the southern portion of the filament was observed by BBSO to destabilize and lose some of its material, and in the morning of August 20th, Meudon H-α observations indicated that the southern portion of the filament disappeared entirely. TRACE observations showed movement of filament material, apparently up to the northeast, and SOHO/EIT saw a dimming, high temperature flare-like brightening (which nonetheless did not have a GOES signature), and a set of loops suggestive of post-flare loops that may have been associated with the filament disappearance (see Table 1 for specific times). However no cusps in Yohkoh/SXT appeared, and no white light CMEs were observed that could be definitely associated with the filament disappearance. Therefore it is impossible to conclude for certain whether filament material was bodily ejected. If it was, it is likely it was only a partial ejection of the flux rope, however, as a faint filament could be seen in the southern portion of the inverse-S-shaped filament channel later in the day (see Figure 1 d, also see Tang (1986)). Note that the northern portion of the sigmoidal filament remained basically intact throughout the disappearance of the southern part.

On the morning of August 21st, SOHO/MDI observed magnetic flux emerging at more or less the same filament mid-point as the magnetic flux cancellation of August 17. This flux emergence continued throughout the day, and was also seen in BBSO H-α observations as an arched filament system (AFS) overlying the emerging flux region (EFR) (see section 3.1 and Figure 5). By the time of Figure 5, the northern part of the sigmoidal filament had vanished. Again it is difficult to determine conclusively whether filament material was bodily ejected: although a white light CME was observed in the NW quadrant, it appeared a little too soon (especially considering it was a slow CME) and was somewhat too narrow (considering the filament was near disk center) to be convincingly related to the filament disappearance, and so may have been an unrelated event originating on the back side of the Sun. Moreover, no obvious SOHO/EIT dimming could be seen (see Table 1 for specific times). As the day progressed, activity continued in the northern part of the sigmoidal region, and included the brightening of an inverse-S-shaped substructure appearing in emission at a range of wavelengths. This will be discussed in more detail in Section 3. Finally, we note that by the end of August 21st, the sigmoidal filament was almost completely gone but the X-ray sigmoid was at its most evident (Figure 1 e).

August 22nd - 26th: remains of the sigmoid. As AR8668 continued on its path to the West limb, it was somewhat more subdued. Yohkoh/SXT X-ray observations showed generally sigmoidal structure, although projection effects made such an identification increasingly difficult. Emerging magnetic flux continued to grow in the mid to northern part of the region, essentially severing the link between the northern and southern parts of the filament, so that a single inverse-S-shaped neutral line no longer existed. Filaments were intermit-

tently apparent along neutral lines to the north and to the south of the EFR (Figure 1 e), and when the region was at the limb on August 26th a prominence was visible in emission, although due to projection effects it is difficult to say if this prominence was associated with our original flux rope or a neighboring magnetic structure.

On August 26 we witnessed the final chapter of our sigmoid observations, as a jet-like CME was observed at the West limb in white light and a range of wavelengths. Interestingly, velocity observations may indicate a twisting of the material in the jet (*Ko et al., paper in preparation*).

2.3. Central questions raised by observations of sigmoidal evolution

We will consider one possible interpretation of the sigmoidal region's evolution in Section 4, but here let us first emphasize a few key questions that are immediately evident from the observations, and which any interpretation would need to address.

1) Although there are several flares and eruptions, the region as observed in X-rays continually returns to a sigmoidal shape. What is the significance of this shape in terms of the energetics of the system, and why is it not permanently destroyed by all the activity?

2) The H-α filament in the region does not appear to be greatly disrupted by the flare of August 17 which temporarily transforms the X-ray sigmoid to a cusp-shape, in fact it become more clearly apparent during and after this activity (also see next question). Pevtsov (2002) showed several other cases of filaments associated with sigmoidal regions that were largely unperturbed by flares and apparent topological changes to the X-ray sigmoid. How is this possible? What does it imply about the relative locations of the filament and the X-ray sigmoid in the general magnetic structure of the region, and their respective evolutions?

3) There is a general trend that when an inverse-S-shaped H-α filament is at its most visible, the X-ray sigmoid is not, and vice versa. In general, the X-ray sigmoid is brightest and best defined during or before periods of significant activity. The filament on the other hand is at its most complete inverse-S-shaped H-α structure during relatively quiescent times. Why does the sigmoidal region appear to move back and forth between active and quiescent periods in the manner observed?

4) The sigmoidal filament is observed in H-α to have its distinct northern and southern portions. The evolution of these two portions have significant differences: they stabilize at different times and also disappear at different times. Moreover, the region between them is the site of both magnetic flux cancellation and emergence. Are these two portions separate

magnetic structures or are they two parts of one larger element? And how is the evolution of the two portions of the filament related to the magnetic flux observations?

5) The August 17 observations of the activity in AR8668 and of the CME to the NE indicate both spatial and temporal connections between the two. How does the activity in the sigmoidal region relate to the larger scale activity of its external environment?

6) The last clear trace of the inverse-S-shaped filament disappeared from the northern portion after two notable changes in the region: first the disappearance of the southern part of the filament during August 20, and second the flux emergence between the northern and southern part of the filament. Could these changes have contributed to a subsequent disappearance of the northern portion of the filament?

7) Finally, on August 21 an inverse-S-shaped region was apparent in many wavelengths, but for most wavelengths was localized to the northern part of the Yohkoh/SXT sigmoid. How is this sub-structure related to the sigmoidal region as a whole, and what caused its brightening?

In order to address the issue of this sub-structure and raise further key questions, we now turn to further observations and analysis of the three-dimensional structure of the sigmoidal region.

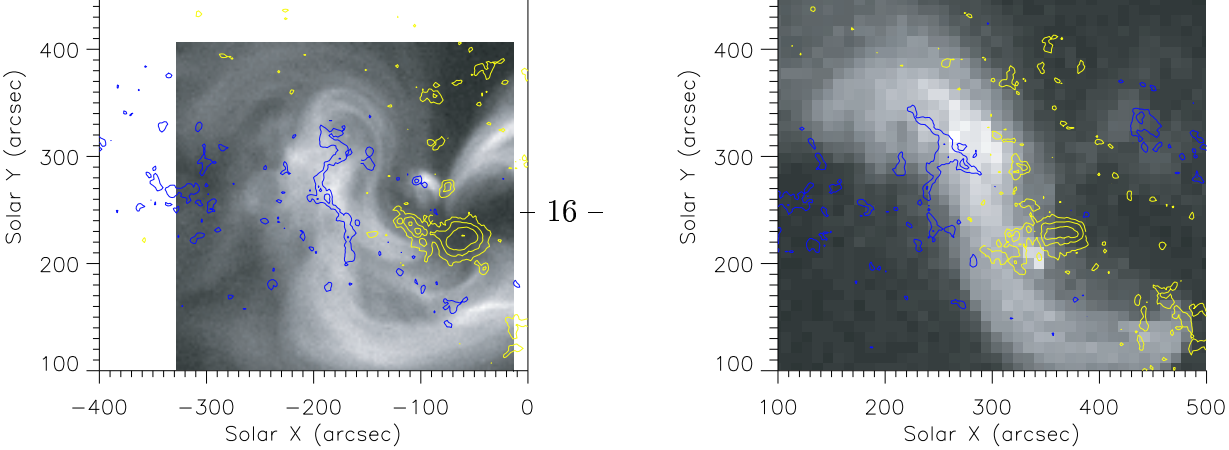

Fig. 6.— Yohkoh/SXT X-ray observations (inverted color table), with contours of MDI observations of magnetic field overlaid (blue: negative, yellow: positive), for a) (left) August 19, 1999, and b) (right) August 21, 1999.

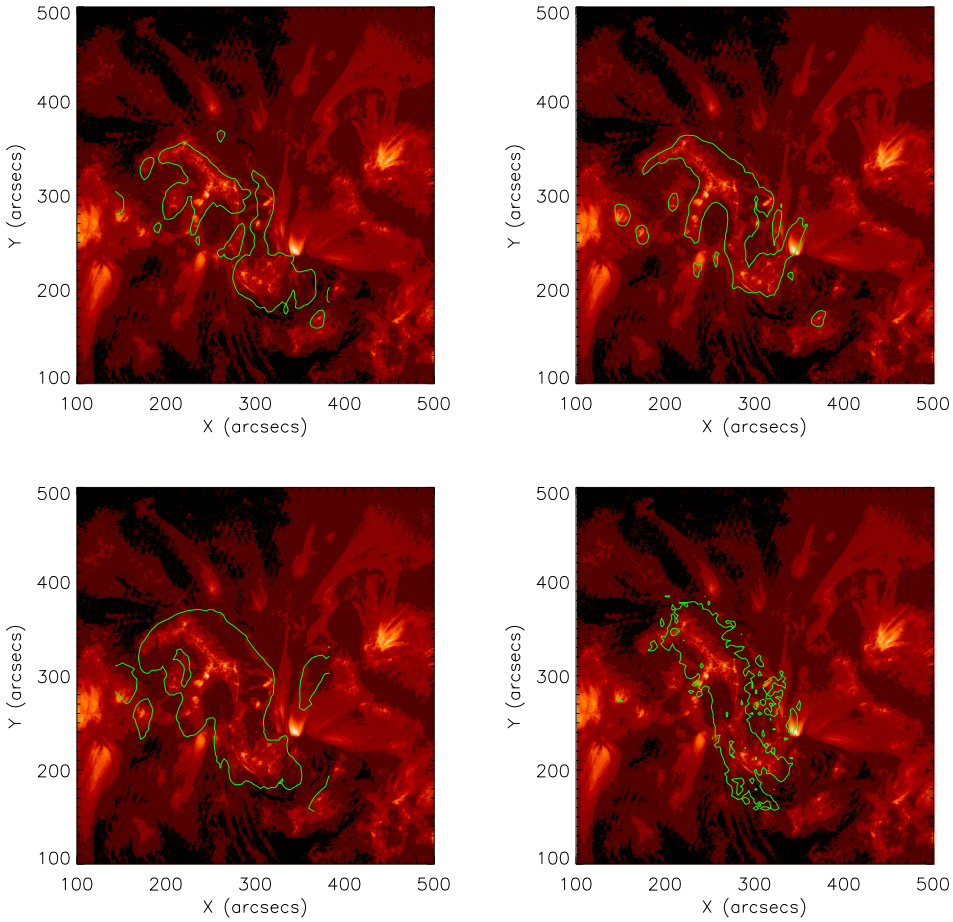

Fig. 7.— August 21, 1999 18:21 UT: TRACE 171 Angstroms EUV observations, with contours of CDS observations overlaid (clockwise from upper left: HeI, MgX, FeXIX, and SiXII.

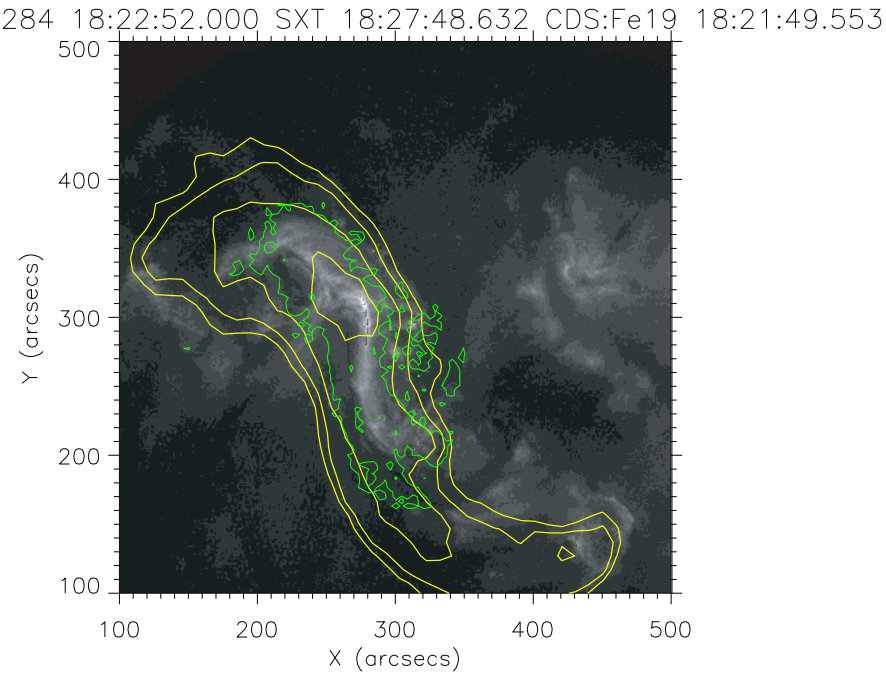

Fig. 8.— August 21, 1999: TRACE 284 Angstroms EUV observations, with contours of Yohkoh/SXT X-ray observations (thick yellow), and CDS FeXIX (thin green) overlaid. Note that the CDS field of view is 4 arc-minutes square, and does not include the area containing the lower half of the super-sigmoid brightening as seen by Yohkoh/SXT.

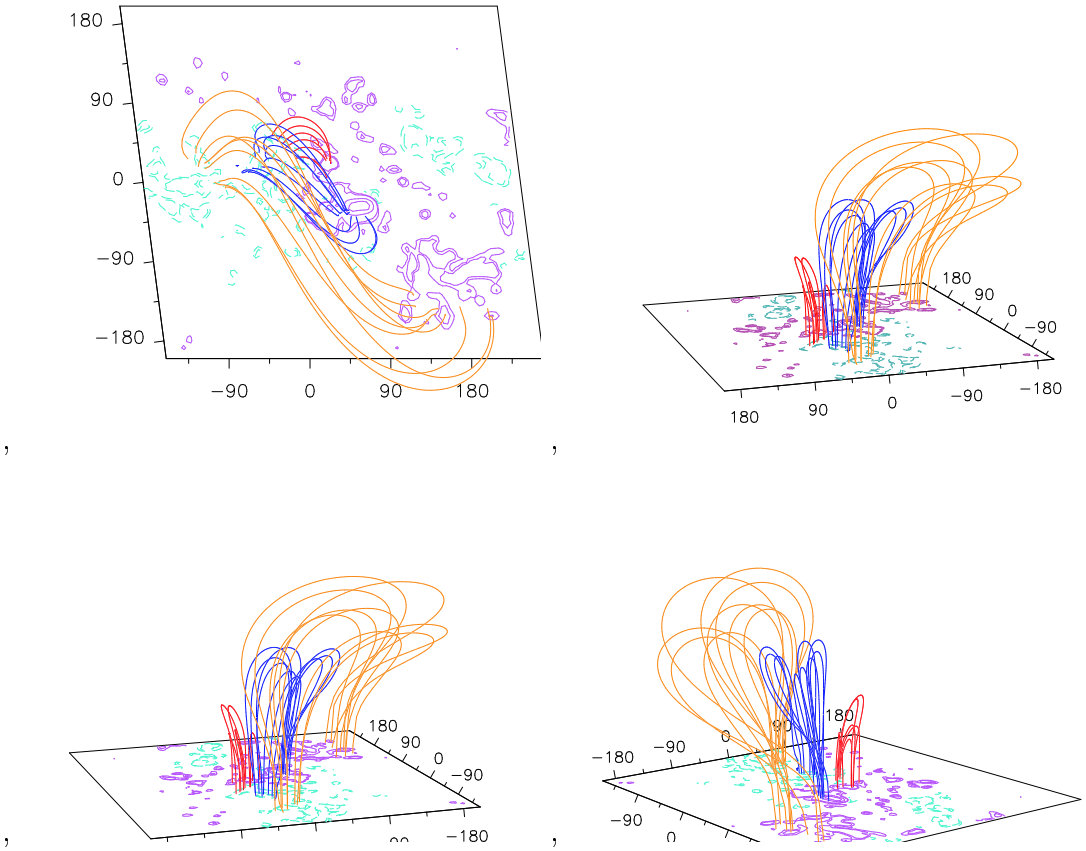

Fig. 9.— August 21, 1999: Linear force-free extrapolation of MDI photospheric magnetic field. The three sets of colored lines highlight three sets of field lines, chosen as best matching the locations of the super-sigmoid (yellow), sub-sigmoid (blue), and emerging flux region (red). The heights (Z) of the field lines have been adjusted slightly so that they can be more easily distinguished: $Z - - > 20Z^{0.5}$. The four views plotted show four different viewing angles to illustrate the three-dimensional structure.

3. Sigmoid structure

3.1. Magnetic complexity of AR8668

An interpretation of a sigmoidal active region as a single group of twisted or sheared field lines implies that these field lines should be rooted in a single magnetic bipole. By overlaying coronal structures on the observed photospheric field we see that this was never the case for our sigmoidal region. Rather, two sets of loops end at two different positive poles: shorter loops connect to the northerly pole centered on the sunspot and longer loops connect to a more diffuse southerly pole (Figure 6 a). It is the longer loops that were generally identified as the X-ray sigmoid throughout its disk passage, although due to projection effects the X-ray sigmoid often was a superposition of both sets of loops. This was the case during the August 21 multi-wavelength brightening (Figure 6 b). However during this brightening the shorter loops were visible at a range of wavelengths (Figures 3, 7), while the longer loops were still clearly visible only in the very hot X-ray emission (Figure 8). Also, the shorter loops manifested a distinctly sigmoidal appearance during the brightening (Figure 2). For clarity and brevity, from here on we will refer to the sigmoid seen in the short loops as the sub-sigmoid, and the original X-ray sigmoid as the super-sigmoid.

One technique that allows us to model the three-dimensional magnetic structure of the entire sigmoidal region is an extrapolation of the photospheric field. We do so under the assumption that there are no significant currents perpendicular to the magnetic field and that any current parallel to the field can be parameterized with a single coefficient for the entire region (i.e. a linear force-free representation). This may not be a very good assumption for a region with such a complex structure, but it is an extrapolation possible using line-of-sight magnetic field observations, and is a first step allowing us to consider how the field might vary with height as well as across AR8668 (see also *Liu et al., paper in preparation* for a nonlinear force-free analysis of AR8668 using vector magnetic field observations). In this manner, Figures 9 a, b, c, d show an extrapolation of photospheric magnetic field observations taken during the multi-wavelength brightening of August 21. Note that the single parameter, α, has been chosen for this extrapolation in order to yield field lines that match the X-ray super-sigmoid (yellow lines). The shorter blue loops were picked out as further inverse-S-shaped loops, and match the location of the northerly sub-sigmoid. The different views of Figure 9 show that this blue sub-sigmoid lies below the yellow loops of the X-ray super-sigmoid. A third set of loops that lies below both of these is also shown (red). These are in the area of the the emerging flux region (EFR) and its associated arched filament system (AFS) as described in Section 2.2 and as seen in Figure 5. Note that the loops of the AFS oriented across the sub-sigmoid can also be seen in the TRACE images (Figure 2a).

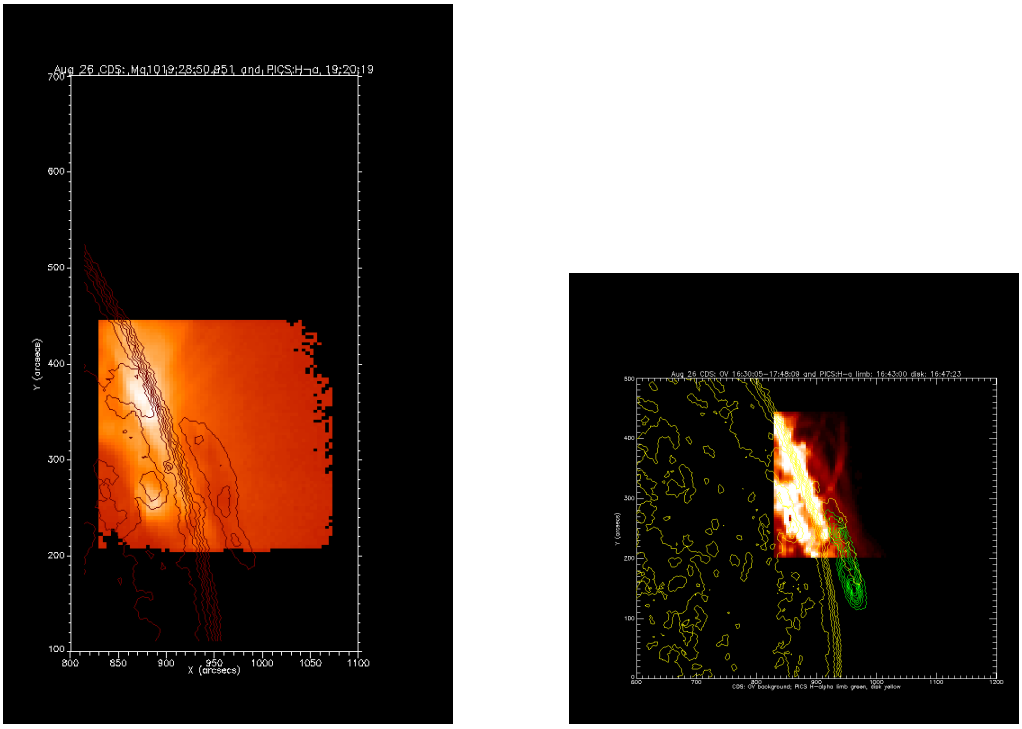

Fig. 10.— August 26, 1999: Observations of AR8668 at the West limb: a) (left) CDS MgX emission (19:28 UT) with MLSO/PICS H-α contours overlaid (19:20 UT), and b) (right) CDS OV emission (16:30 UT) with MLSO/PICS H-α contours overlaid (16:43 UT).

The identification of the upper, yellow magnetic loops with the Yohkoh/SXT super-sigmoid and the lower, blue magnetic loops with the multi-wavelength sub-sigmoid brightening is tempting, but we need to be careful. It is important to consider what exactly the different wavelengths are showing. We refer to short "loops" forming the basis of this brightening, but in fact not all of the wavelengths are showing loops - some are presumed to show only the footpoints of loops. Studies of TRACE observations have identified finely-structured EUV emission at the level of the chromosphere/transition region, associated with overlying Yohkoh/SXT loops, which has been termed "moss", due to its intermittent, spongy appearance (Berger et al. (1999); Fletcher and De Pontieu (1999)). Figure 7 shows TRACE observations at 171 angstroms, which primarily pick out the low altitude (chromospheric) moss in the sub-sigmoid. The overlays of the SOHO/CDS lines imply that all but the hottest lines (SiXII, FeXIX - sensitive to, respectively, 2 million and 8 million K material) are mostly showing this moss. This is borne out by considering observations of the region at the West limb. (Although there is probably significant evolution between the multi-wavelength brightening of August 21 and AR8668 once it has reached the limb, the limb observations may still provide insight into the region's structure with height.) Figure 10a shows MgX emission at the limb, overlaid with contours of H-α showing a prominence. Although there appears to be some higher altitude coronal emission in MgX to the north, the brightest portion of the MgX emission lies below the height of the prominence that can still be seen to the south. The emission coming from moss thus may generally overpower loop emission for the lines sensitive to material at about a million Kelvin. This does not mean coronal loops do not exist at these temperatures. Although the brightest MgX emission lies below the prominence, Figure 10 shows that loops to the north are still visible. But for the on-disk observations, it is only during transient brightenings such as on August 21 (e.g. 2) that the EUV emission shows loops that make up a clear sigmoidal pattern.

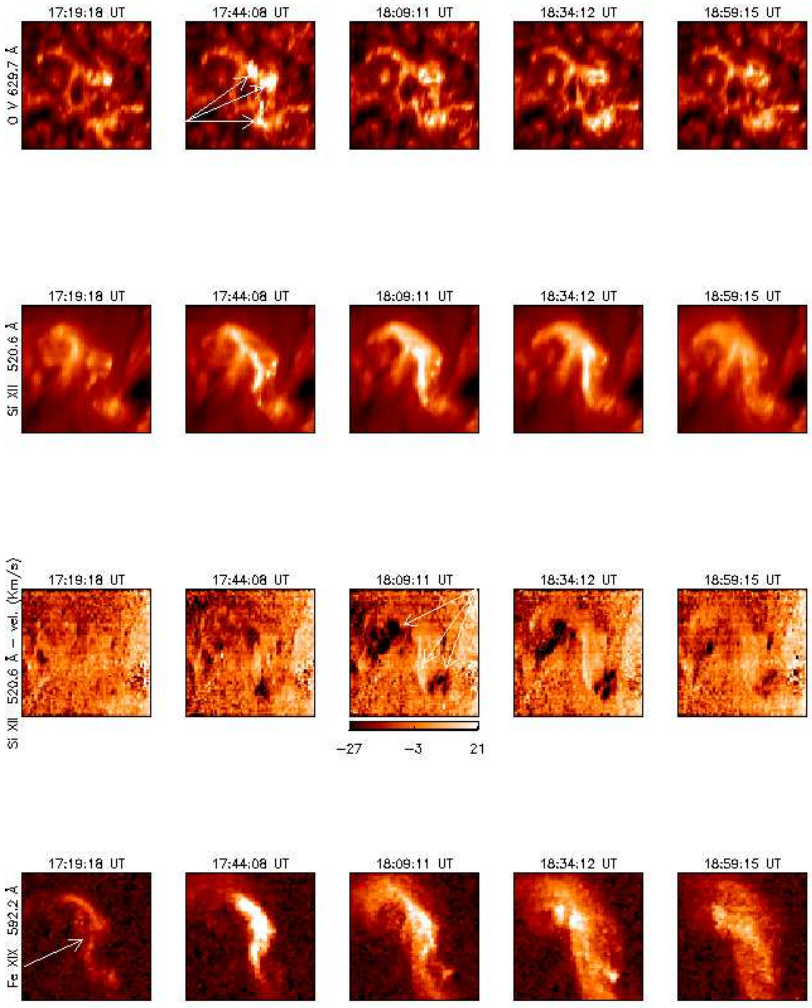

Fig. 11.— A sequence of CDS rasters, showing the sub-sigmoid brightening (not GOES classified) at 17:44 UT, August 21. From top to bottom: monochromatic images of OV (transition region), SiXII (upper corona), velocity map as derived from SiXII line profiles (dark implies up-flow), and images of the FeXIX line. All line intensity images in a row are plotted with the same intensity scale. The third row shows velocity maps, with the velocity scale in km/s illustrated under the central image. The central time of each raster is indicated. Arrows point out the small flare-like brightening in the second OV raster, the downward (bright) and upward (dark) flows in the third Si XII velocity raster, and the sigmoidal precursor in the first Fe XIX raster.

3.2. Sigmoid structure in temperature, density, and velocity

The temperature structure of AR8668 can generally be determined by looking at which parts of the structure emit in which lines. Line ratio diagnostics can also be used to attempt to pin the temperature down more precisely. Del Zanna et al. (2001) considered SOHO/CDS temperature diagnostics of AR8668 just prior to the August 21 multi-wavelength brightening. The CDS lines did not show an obviously sigmoidal shape at this time, but more diffuse emission from SiXII and FeXVI lines implied that some plasma of two-million degree temperature was present prior to the brightening, as is the case for most active regions. A lack of emission in FeXIX implied that there was not much plasma at temperatures above a few million.

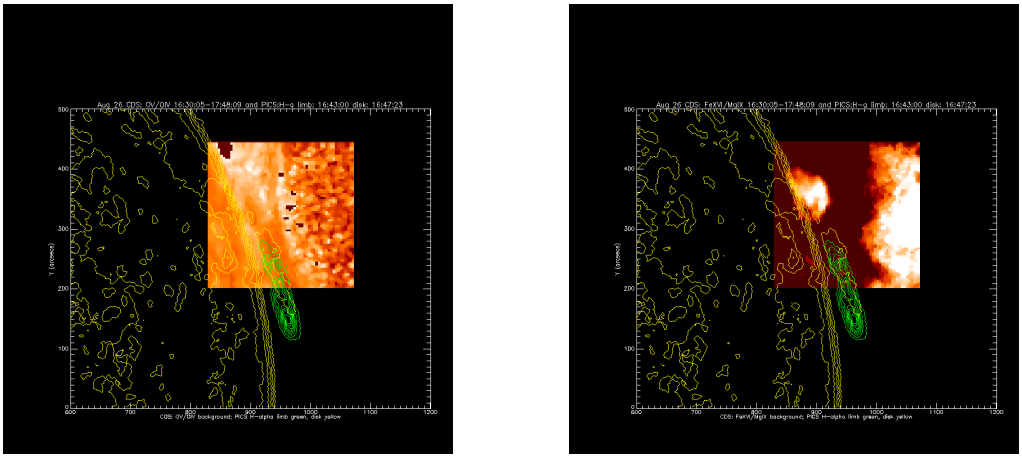

Fig. 12.— August 26, 1999: Observations of AR8668 at the West limb: a) CDS OV/OIV temperature line ratio (cooler material) with MLSO/PICS H-α contours overlaid, and b) CDS FeXVI/MgIX temperature line ratio (hotter material) with MLSO/PICS H-α contours overlaid.

Although very little FeXIX emission was present before the brightening, as the brightening began, a clear sigmoidal shape formed first in FeXIX (Figure 11). This implied heating to at least 8 million Kelvin. The fact that FeXIX, or any of the other SOHO/CDS lines, did not show sigmoid loops prior to this implies that the X-ray sigmoid plasma had been at at a temperature between 2 and 7 million Kelvin, since the SOHO/CDS lines used in this study lay either below 2 MK or above 7 MK. The small flare-like brightening (not GOES classified) centered on the EFR loops then appeared, and emission spread out from this brightening until a clear sigmoidal structure was lit up in the CDS lines. The hottest FeXIX emission appeared as a sigmoid aligned with the super-sigmoid seen in Yohkoh/SXT. The CDS field of view is only 4 arc-minutes square, and so shows the northern part of AR8668. Thus it is certainly possible that the FeXIX emission shows the top half of this super-sigmoid (Figure 8). The cooler temperature lines (including TRACE) show the sub-sigmoid oriented at an angle to the super-sigmoid. There is essentially a clockwise rotation between the sub- and super-sigmoids, from cooler to hotter (Figure 3).

We also analyzed plasma diagnostics from SOHO/CDS for the region once it had reached the West limb. Figure 12a shows the ratio of OV to OIV emission, a diagnostic sensitive to cooler (around $1 - 3 \times 10^5$ Kelvin) material, while Figure 12b shows FeXV/MgXIX, a diagnostic sensitive to hotter (around $1 - 3 \times 10^6$ Kelvin) material. From these we see that the hotter material lies above the cooler material, consistent with the magnetic field extrapolation where the super-sigmoid loops lay above the sub-sigmoid.

Velocities were also calculated during the August 21 event, showing significant (around 30 km/sec) blue shift at both ends of the sub-sigmoid implying up-flow of 1-2 million degree coronal plasma (Figure 11, third row). Red shifts were also seen, implying down-flow, primarily along the spine of the sub-sigmoid, both in coronal plasma, and also to a lesser extent in cooler (OV line shifted) plasma. More down-flow of material was seen at the ends of the sub-sigmoid in both coronal and transition region lines after the event. TRACE movies also show up-flow and down-flow of material during and after the event.

Densities were calculated prior to the brightening, and were found to be in the range $1 - 3 \times 10^{10} cm^{-3}$ for transition region values (from the O IV 629.9/554.5 Angstrom ratio) and about $3 \pm 1 \times 10^9 cm^{-3}$ for coronal temperatures (from the SiX 347.3/356.05 Angstrom ratio). The exception was in the region of the bright EFR loops, where densities reached $6 \times 10^{10} cm^{-3}$. During the sigmoidal brightening, densities greater than $10^{11} cm^{-3}$ were found using the OV/OIV line ratio. Finally, comparing diagnostic observations from just before and just after the event, del Zanna et al. (2001) found that for the plasma around one million Kelvin there was no obvious change in overall densities and temperatures.

3.3. Central questions raised by observations and analyses of sigmoidal structure

These observations and analyses give us information about the sigmoidal region's structure in general, and in particular during the August 21 multi-wavelength brightening. This allows us to expand on some of our earlier questions, as well as to raise a couple of new ones and so continue our list of questions:

8) The magnetic field extrapolation used in Section 3.1 was useful for getting an idea of how the observed X-ray and multi-wavelength loop brightenings might relate to the field and to each other in three dimensions. However, it is a simple extrapolation using line-of-sight fields. How realistic a representation is it really? In particular, where does the filament fit into the magnetic field structure?

9) The brightening appeared in a range of wavelengths signifying material emitting at a range of temperatures. Many of these wavelengths only showed a clear sigmoidal structure during this brightening. (This was also the case found by Sterling et al. (2000) – i.e. sigmoids generally appeared in EUV emission only during heightened activity such as flares.) Why were pre-brightening sigmoidal structures only apparent in hot X-ray or cool filament temperatures? Either there were no sigmoidal loops present at EUV-emitting temperatures, or any pre-brightening EUV loop emission must have been very faint - so faint to be generally not separately detectable against diffuse coronal emission from the surroundings and moss emission from below. Either way, the question is what changed during the transient brightening on August 21 so that sigmoidal loops became visible in EUV?

10) Although a system of short loops connecting to the northerly positive pole appear to exist well before the transient brightening (e.g. Figure 6a), during the brightening these loops have a distinctly sigmoidal, and even tube-like appearance (Figure 2). How does this sub-sigmoid magnetic structure relate to the overlying X-ray sigmoid, and to the emerging magnetic flux that is observed before, during, and after the transient brightening?

11) SOHO/CDS observations showed that the small brightening, which preceded the appearance of the sub-sigmoid at multiple wavelengths and the velocity up-flows, originated in the region of the new emerging magnetic flux (see e.g. OV images of Figure 11). In addition, a FeXIX inverse-S-shaped precursor was visible possibly even before this EFR-centered brightening. What caused these three features (precursor, brightening, and up-flows), and what might be the significance of their relative locations and timing?

12) What do the high transition region densities during the brightening imply?

13) Overlaying the emission from the various CDS lines observed during the brightening

shows an apparent rotation of structure with wavelength/temperature, i.e. clockwise from cooler to hotter material (Figure 3). Observations of the region at the limb and identification of structures with extrapolated magnetic field lines implies that the hotter material lies at higher altitudes: does this then mean that there is an overall twisting or shearing of the sigmoidal structure with height? Gibson et al. (1999b) reported evidence of a similar rotation with wavelength for a different sigmoidal region: in that case the rotation appeared counterclockwise from cooler to hotter material, but for a forward S rather than a backwards S. Could this rotation of sigmoidal structure with temperature (and possibly height) be an indicator of the global direction of twist, or magnetic helicity in the region?

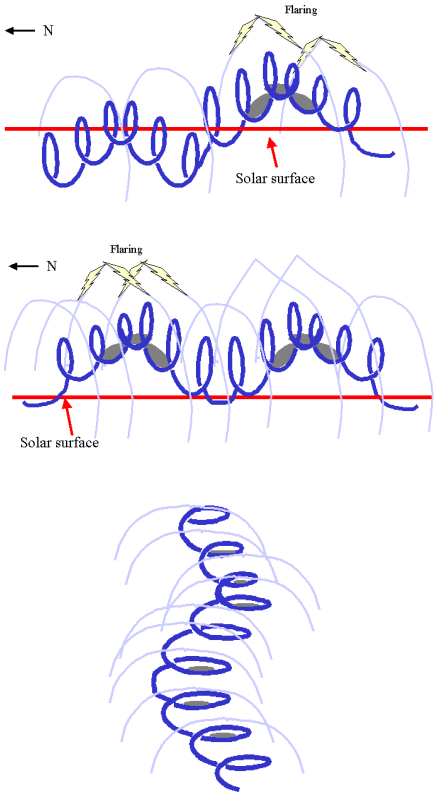

Fig. 13.— Cartoon representation of bent flux rope emerging through a solar surface. Top: southern part of flux rope emerges, accompanied by flaring. Middle: northern part of flux rope emerges, accompanied by flaring. Bottom: same as middle, but viewed from above. Grey shading represents filament material. Note that this cartoon represents a highly twisted rope in order to emphasize its structure: the real system may contain a significantly smaller amount of twist (see discussion in text).

4. Interpretation

Let us now suggest one interpretation, describing the emergence, equilibration, and ultimate disruption of a twisted magnetic flux rope structure, against these observations. We do not claim this is the only possible explanation of the observations, but it does succeed at addressing the key questions of the observed sigmoidal structure and evolution - something any interpretation put forward needs to do. Questions that are so addressed are referred to in parentheses after the relevant points.

A twisted magnetic flux system emerges from beneath the photosphere into the corona forming the basis of AR8668. We expect some minimum amount of preexisting twist in the magnetic structure as it emerges through the photosphere, for the following reasons. It has been found that a minimum amount of twist is needed to ensure that flux tubes rise cohesively through the convection zone (e.g. Emonet and Moreno-Insertis (1998); Fan et al. (1998); Abbett et al. (2000, 2001)). Moreover, vector magnetogram observations imply that this twist is still there when magnetic structures emerge through the photosphere (e.g. Leka et al. (1996); Tanaka (1991)). We would expect, however, that even if a magnetic structure similar to our highly simplified cartoon representation of Figure 13 exists sub-photospherically, its form will probably be altered as it passes through the photosphere. For example, Fan (2001) showed using a numerical MHD simulation that the weight of entrained material in an emerging flux rope could stop it from smoothly rising into the corona intact. We therefore expect that that the rising magnetic flux system will undergo significant alterations via reconnections as it moves into the corona. However, even though the magnetic field and associated currents would be altered by such reconnections, the magnetic helicity of the system must still be conserved (see Berger and Field (1984); Low (1994) for discussion of magnetic helicity conservation). As long as there is any helicity in the system at all, there must also be some currents and magnetic energy: this magnetic energy is essentially trapped by the conservation of magnetic helicity. (Please see Low (1996,1999) for further discussion.) Note that we make the assumption that the helicity of our emerging magnetic structure stays more-or-less local to it, which is consistent with the observation that the sigmoidal structure is maintained. The flux rope thus undergoes reconnection within itself as well as reconnections with the external coronal field that it emerges into, until it has reached a metastable equilibrium state possessing a lowest possible energy that still conserves helicity. It is this equilibrium state that we represent as a twisted, rope-like structure (akin to a slinky) suspended in the corona in Figure 13. (Question 1).

The observations of large flares and filament formation on August 16-17 are then the manifestation of the flux rope emerging, reforming, and equilibrating with its external environment. The sigmoid as seen in X-rays shows the interface between the field lines twisting

around the rope axis and the external (non-twisting) fields (Figure 13c). This is essentially a magnetic "separatrix", which generally refers to a surface across which the linkage of magnetic field lines is discontinuous. In classical electricity and magnetism theory, such surfaces in 3-d originate from magnetic null points, from which field lines diverge. Quasi-separatrix layers, or QSLs, extend this concept to refer to layers of finite thickness across which the field connectivity changes abruptly (Priest and Démoulin (1995); Démoulin et al. (1996)). These layers are natural location for tangential discontinuities and current sheets to form during dynamic evolution of the system, where reconnection and dissipative heating can then arise (Parker (1987); Low (1991); Démoulin et al. (1996)). Therefore, we will refer to the X-ray sigmoid as a QSL occurring where neighboring field lines on either side have significantly different paths, leading to widely separated endpoints (i.e. winding vs. non-winding lines). During its emergence and reformation, the rope expands upwards against the external fields. The resulting heating from reconnections between tangentially discontinuous field lines illuminates the sigmoid QSL. Depending on the details of the rope vs. external field topologies as well as the driver mechanism, this reconnection may lead to an explosive flare, or alternatively yield a more gradual heating. Internal reconnections that act to reform the rope in the corona (such as that described in Démoulin et al. (1996)) also contribute to the overall sigmoidal shape. Reconnections along the surface layer and throughout the volume defined by the QSL continue until a minimum energy state is reached and an emerged (reformed) rope can exist in metastable equilibrium. Such equilibrating flares and brightenings are not necessarily indicative of a major ejection of the flux rope, but rather may be reconnections acting to redistribute (but not remove) magnetic helicity within the system and dissipate as much energy as possible while conserving magnetic helicity. Thus the basic geometry of the QSL (to first order an inverse-S-shaped surface) is largely unchanged throughout the region's disk passage and reappears whenever there is significant heating within and along the rope due to further reconnections as the rope evolves and is forced to form new equilibria with likewise evolving coronal conditions. (Questions 1, 2, 3).

The minimum energy configuration (i.e. flux rope) is a magnetic environment which can contain a filament – the filament material is supported by magnetic forces, as it sits in the dips that are the bottoms of the winds of the flux rope (Rust and Kumar (1994); Aulanier and Démoulin (1998); Gibson and Low (1998)). Note that the magnetic field presented in Figure 9 above, most likely due to its simplicity as a linear force-free extrapolation of line-of-sight magnetic fields, does not yield a magnetic environment having dips that would support a filament. An extrapolation that uses a spatially varying force-free field parameter α and vector magnetogram observations of our sigmoidal region does show dipped magnetic field configurations, however (*Y. Liu, private communication*). Nevertheless, neither extrapolation yields a highly wound structure as seen in our cartoon of Figure 13. Although the

uncertainties in both the magnetic field observations and in the techniques used to extrapolate them mean we cannot rule out such a highly twisted structure, it has been argued that such a tightly wound flux rope is prone to instabilities and eruption: a stably existing rope may be more likely to contain significantly less twist (closer to one full turn) (see e.g. Rust and Kumar (1996)). However, additional constraining effects such as the weight of filament mass within the rope could counteract this instability and allow a metastable equilibrium even for a highly wound structure. Thus the presence of the high degree of twist would be an effective storage device for magnetic energy, and an eruption of the rope could easily be triggered if the filament weight were significantly altered, leading to a loss of equilibrium (see Low (1999)). The degree of twist that could exist within CME precursors and role of filament mass in CME energetics remain interesting open questions. (Questions 2, 8).

It is useful, for our interpretation of AR8668, to consider the flux rope to have a bend in its middle (vs. height), and to have the southern part finish its equilibration with the background corona first (Figure 13a-b). The bend in the middle effectively keeps the northern and southern portions of the rope magnetically distinct until the full emergence (or reformation) of the rope: field lines are tied to the photosphere and so the two portions equilibrate with the external environment separately. (An interesting question this provokes is how such a bend might arise – see for example (Linton et al. (1999); Fan et al. (1999)), for a description of how the excitation of multiple unstable modes during a flux tube's convective rise through the photosphere produces compact kinks at a flux tube midpoint.) As the top of the flux rope pushes against the external field, reconnecting and flaring (Figures 1a, 13a), the magnetic field structure in the southern part of the rope reaches a metastable equilibrium state where the filament can remain quiescently in bottoms of the winds of the southern part of the rope. The northern part of the rope lying above the photosphere is magnetically separate from the southern portion of the rope above the photosphere at this time, and has not reached its own equilibrium yet – in the cartoon it has not itself fully emerged. As it does emerge, reform, and reach its own equilibrium, it also manifests the pattern of flaring followed by filament stabilization (Figures 1b, 13b) corresponding to internal and external reconnections, followed by the appearance of a filament sitting in the bottoms of the reformed flux rope winds. The magnetic flux cancellation that occurs as the northern part of the filament stabilizes (Figure 4) might be interpreted as the actual emergence of the central bend of the flux rope, as the U-shaped bottoms of the magnetic flux rope manifest as an apparent magnetic flux cancellation (see Figure 13b and Spruit et al. (1987); Low (1996); van Driel-Gesztelyi et al. (2000)). Another interpretation, consistent with the idea that the rope is reforming in the atmosphere, was presented by Chae et al. (2000), who cited AR8668 BBSO H-α observations of diverging flows and up-flows of cool mass at the location of the magnetic flux cancellation as evidence of of an ongoing reconnective process (van Ballegooi-

jen and Martens (1989)) and an associated upward transport of filament material (Rust and Kumar (1994)). It is possible that the stretching caused by upwards expansion of the top of the flux rope has led to a reconnection across the dipped magnetic field lines weighed down by photospheric material, with a subsequent lifting of a lighter load of filament material into the corona. (Questions 2, 4).

The flares of August 16th and 17th are thus stabilizing, rather than destabilizing effects on the flux rope and its associated filament. Although on August 17th there is a clear sigmoid-to-cusp transition above the northern part of the filament channel and associated post-flare loops, there is no clear evidence that filament material is ejected; in fact the northern part of the filament becomes clear immediately after this flare (see also Pevtsov (2002)). We interpret this to mean that this flare, like the others on August 16th and 17th, is part of the equilibration process – if any of the flux rope erupts, it does so only partially and in a manner that leaves the rest of the flux rope behind in a metastable equilibrium allowing the filament to continue to grow (see e.g. Tang (1986) and Figure 3 of Gilbert et al. (2001)). However, the neighboring streamer/polar crown filament does erupt in a large CME. This is not surprising, as the equilibration between AR8668 and surrounding fields affects the configuration of the external field as well as that of AR8668 (an interesting analysis of how emerging magnetic flux at a given latitude can cause CMEs to erupt at a significantly removed latitude can be found in Zhang and Low (2001)). Conceivably the streamer to the NE may have been in an energetic state, ready to erupt, so that the first August 17 flare in AR8668 (with a peak at 13:23 UT) provides perturbation enough to trigger it. The second flare (with a peak at 16:02 UT) and X-ray cusp formation shows the magnetic field reconnecting behind that CME and/or perhaps a partial ejection of the flux rope of AR8668. The flux rope is then left in metastable equilibrium. (Questions 2, 5).

The rope is now in a relatively stable, presumably minimum energy configuration (for a given magnetic helicity), and the filament continues to grow. This is the observed behavior of August 18-19. At the same time the X-ray sigmoid is less evident, since the system is relaxed and no longer reconnecting much within itself or with its environment, and so the QSL is only minimally heated (although the QSL still exists, and presumably still has a sigmoidal shape). Thus the X-ray sigmoid is apparent during the activity associated with equilibration between the flux rope and coronal environment, and the filament is at its most apparent during the resulting metastable equilibrium state. During this period, however, motion in the southern part of the sigmoidal filament increases, until on August 20 the southern part of the filament completely disappears. It is possible that it is at least partly ejected, taking with it a portion of the flux rope's stored-up magnetic helicity. It is interesting to note that the dimming seen by SOHO/EIT precedes the disappearance of the southern part of the filament: this might imply that the overlying coronal arcades open up, removing

a necessary constraint on the region's metastable equilibrium, so that the flux rope then erupts outwards. The entire flux rope is not ejected, however, and the northern portion of the filament remains. By the morning of August 21 the northern part of the filament also disappears (possibly in another partial ejection). New magnetic flux is observed to emerge near the filament's midpoint prior to the disappearance of the upper portion of the inverse-S-shaped filament. Such emerging flux may significantly affect the lower boundary condition of the original flux rope, and in so doing redefine what is a minimum energy for the system, or in some other manner destabilize the rope (see e.g. Raadu et al. (1988)). The effect of the emerging flux, along with the lightening of the gravitational anchor of the southern part of the filament as well as the possible ejection of some of the rope's helicity with the the southern part of the filament, may be the key factors in completely pushing the flux rope out of its metastable equilibrium. (Questions 3, 6).

As these effects push the system once again into a period of instability, the X-ray sigmoid structure is at its most obvious. It is at this point also that the sub-sigmoid becomes temporarily apparent at a range of wavelengths. We interpret this sub-sigmoid brightening to arise due to tangential discontinuities and reconnections along the QSL that lies between the bottom of the original flux rope and the new EFR that pushes up from below. The first manifestation of the multi-wavelength brightening is the appearance in FeXIX of a sigmoidal structure, aligned, however, with the Yohkoh/SXT super-sigmoid. The FeXIX precursor may indicate heating along the upper QSL, as the original flux rope is pushed up against the external fields by the emerging flux below. The small brightening is then visible at the sub-sigmoid QSL centered on the EFR, and velocity up-flows are observed at the endpoints of the sub-sigmoid. The sub-sigmoid begins to appear at a range of temperatures because the flare-like heating has caused chromospheric evaporation of enough material to coronal heights so that enhanced emission can be observed at a range of temperatures along the sub-sigmoid QSL. Specifically, chromospheric material is evaporated causing the up-flows observed by SOHO/CDS (see also Czaykowska et al. (1999)). At the same time some cools down and falls back down (SOHO/CDS red-shifts), and in so doing increases transition region densities. The increase of density in the sub-sigmoid loops means that there is enough material there to be seen at 1-2 million Kelvin as the flare-heated plasma cools down. The super-sigmoid, however, never shows up brightly at wavelengths other than the very hottest because it is both longer and higher than the sub-sigmoid, so that the density of evaporated material at 1-2 million Kelvin is much less. Such an inverse relationship between brightness and loop length during flare activity has been observed both for sigmoidal and non-sigmoidal loops (Manoharan et al. (1996); Gaizauskas et al. (1998); Mandrini et al. (1996)). Thus, sigmoids may not be generally apparent at wavelengths other than soft X-ray because ordinarily there is not enough material at EUV temperatures in the sigmoidal loops to be

easily visible, particularly against the strong background EUV emission from chromospheric moss. Because SOHO/CDS and TRACE happened to be observing during the flare and with a high time cadence, they caught the brightening of the sub-sigmoid at a range of wavelengths while densities in the sub-sigmoid were high. The super-sigmoid is apparent both before, during, and after the sub-sigmoid brightening at soft X-ray temperatures, because enough plasma is sustained at soft X-ray temperatures to show up easily against an otherwise dark background. However note that the super-sigmoid is most clear during the brightening, as it too responds to the input of energy from the small flare. (Questions 3, 7, 9, 10, 11, 12).

We have not explicitly modeled the magnetic configuration of our flux rope and the QSL associated with it. One possible topology has been presented by Titov and Demoulin (1999). This model predicts upper and lower QSLs, akin to the observed sub- and super-sigmoid. Work is being undertaken elsewhere (*Canfield et al., paper in preparation*) to explicitly compare predictions of the Titov and Demoulin (1999) model to observations of AR8668. However, the Titov and Demoulin (1999) topology does not include or require the EFR for the appearance of the lower QSL. Observations of the multi-wavelength sub-sigmoid brightening of August 21 imply that the small flare that triggered the brightening is located at the EFR. It is possible that the lower QSL existed throughout the disk passage of AR8668 (note for example the lower loops visible on August 19 in Figure 6a), and that the role of the EFR pushing up from underneath is primarily squeezing magnetic fluxes together, causing tangential discontinuities in the field and subsequent reconnections along the rope's QSLs. It may in the process transfer some of its helicity to the flux rope above it, so that the lower QSL takes on a clearly sigmoidal appearance. We have analyzed vector magnetogram observations from Huairou solar observing station, and found that they indicate the same sign (negative) of current helicity for the original sigmoidal fields and the EFR (the method to calculate the helicity and the definition of the sign of the helicity are as described in Abramenko et al. (1996). As defined in that paper, the imbalance ρ of current helicity is -21% for AR8668 as a whole, -29% for the central positive polarity (sunspot), and -21% for the emerging flux region.). Thus the emergence of the new magnetic flux could add to the twist in the original flux rope (see e.g. Canfield and Reardon (1998); Moore and Roumeliotis (1992)) and so compensate for magnetic helicity lost in the ejection of pieces of the filament. Indeed, the apparently separate magnetic flux systems of the original flux rope and the EFR could actually be two outbreaks of a single complex sub-photospheric flux rope. The twisting of the combined system with height as seen by the SOHO/CDS lines in Figure 3 may be a result of the single shared direction of twist (for example such a rotation of field lines with height was described for a CME spheromak-type flux rope model in Gibson and Low (2000). (Questions 1, 10, 13).

As a final comment, we note the almost too apt symmetry of the evolution of our

sigmoidal region. It appears to be in a process of formation as it first becomes visible in the Eastern hemisphere, then, at central meridian the filament is at its largest and most stable, and then, as it moves towards the Western limb, it loses stability and decays. We seem to witness birth, maturity, and death. Although ultimately every active region does go through these three stages, we do not necessarily think that the full process was viewed in the disk passage of AR8668. Rather, the evolution of the system was more of a binary one, alternating between stability and the activity necessary for its re-equilibration. As new flux emerged and the global coronal field evolved, the metastable equilibrium was disrupted, and the region went through brightenings and eruptions until once again stability was obtained (note the lack of flares/brightenings and eruptions on August 22-25). It is impossible to definitely say whether the region is still sigmoidal when it has reached the limb, since projection rules out an X-ray sigmoid identification. However, the fact that the region is still active (as evidenced by the jet of August 26) implies that the region still may have energy stored up in magnetic helicity, and be going through another phase of equilibrating with its environment. (Question 3)

5. Conclusions

The observations outlined in this paper represent the most comprehensive study to date of a sigmoidal active region. By considering observations at multiple wavelengths that span the full passage of the region across the solar disk, we have gained new insight into the structure and evolution of sigmoids, and encapsulated the outstanding issues raised by observations into a list of physical questions that need to be addressed in any theoretical interpretation.

One such question is raised by the observation that a clear S shape is generally only visible in the very hot X-ray images or the relatively cool H-α filament images, but does appear at 1-2 million Kelvin during events such as the August 21 brightening. We suggest that this hinges upon the density in the loops: when chromospheric evaporation supplies enough hot, dense material to the short loops of the sub-sigmoid region, these become visible in intermediate temperatures as they cool down. The super-sigmoid remains largely invisible in the intermediate temperature plasma, as an equivalent energy input yields a much lower density in the high, long loops. In between flares or flare-like brightenings, slow or bursty reconnection heating may not be energetic enough to evaporate sufficient material to any of the sigmoidal loops for 1-2 million degree plasma to appear against its background emission, and so only the X-ray sigmoid can appear, as a significantly lower density may be adequate for X-ray loops to be visible against their relatively dark background.

The hypothesis that a sigmoid's manifest twist leads to a region likely to erupt is borne out by the observations. We have presented an interpretation of the sigmoid's evolution as the emergence of a flux rope, where the filament rests within the bottom of the winds of the rope, and the X-ray super-sigmoid appears at the quasi-separatrix layer between the rope and external fields. As new emerging flux pushes up underneath the original flux rope, a sub-sigmoid appears at the QSL between the emerging flux and the super-sigmoid. Various flares and brightenings are common at these QSLs, but the energy stored in the twist of the flux rope is not shed during these dissipative events, and so the flux rope structure is not greatly changed (as is directly implied by the observed lack of change in density and temperature after the August 21 brightening). The primary mechanism for ultimately shedding the sigmoid's twist and its associated energy may well be bodily ejection into interplanetary space by a CME (Low (1994)), but there is no evidence in our observations of the complete ejection of the flux rope structure: rather it appears that the rope undergoes multiple partial ejections as reconnections release one piece at a time (Tang (1986); Gilbert et al. (2001)). Emerging magnetic flux also continues to input magnetic helicity into the region. This has been discussed for the easily identified EFR associated with our region on and after August 21st, but could also occur as tiny EFRs with associated twist transfer their helicity from their own smaller scale to the larger scale of the sigmoid flux rope: MHD turbulence tends to drive magnetic helicity from small to large scales. Thus the paradox of the sigmoid being both active and robustly recurrent is resolved: it is intrinsically energetic in its interaction with its surroundings, but not itself easy to destroy as the helicity that maintains its sigmoidal interface is continually replenished via emerging magnetic flux and only partially removed through ejections.

Of course our interpretation does not succeed in explaining all of the observed behavior of AR8668, and indeed has raised many questions which are incentive for future studies. For example, we have described the filament material as stably resting in the bottoms of winds of a slinky-type flux rope, but observations show material moving back and forth along the axis of the filament. This might be explained in terms of a sloshing back and forth of the flux rope (and so an apparent axial motion of material which actually does not move out of its local "dip"), but may also point to a steady-state of the filament where material is in constant motion along the filament, in and out of local dipped regions of the magnetic field. (See Gilbert et al. (2001) for an interpretation of apparent helical motions along a filament (consistent with a flux rope model), and Karpen et al. (2001) for a discussion of whether dipped fields are necessary in a dynamic filament environment.) Further analysis of observed filament velocities for AR8668 might clarify this issue.

In conclusion, we feel that we have presented a physical interpretation which successfully addresses enough of the observed phenomena to make it plausible, and crucially allows us

to step back from the details of the observations and view the fundamental processes that they illustrate.

We would like to acknowledge the following people and sources: B. C. Low for helpful discussions, Y. Fan for internal NCAR review of the paper, Y. Guo for assistance with the BBSO data, S. Martin and P. Zink for comments during the WSM3 campaign, the SOHO/CDS team, and the LASCO daily movie page at *http : //lascowww.nrl.navy.mil/daily_mpg*. The Yohkoh SXT project is a collaborative project of LMSAL, the National Astronomical Observatory of Japan, and the University of Tokyo, supported by NASA and ISAS. TRACE is operated jointly out of Goddard Space Flight Center by scientists from the University of Chicago, Montana State University, LMSAL, and the Harvard-Smithsonian Center for Astrophysics. SOHO is a project of international cooperation between ESA and NASA. Part of SEG's work was done while visiting the Dept. of Applied Maths. and Theo. Phys. at the Univ. of Cambridge. LF acknowledges support from NASA grants NS8-37334 (SXT) and NAS5-38099 (TRACE), and from a PPARC Standard Astronomy Grant. HEM and GdZ also acknowledge financial support from PPARC. C. M. acknowledges support from the Carrera del Investigador Científico, CONICET, Argentina, and C. M., B. S. and P. D. acknowledge financial support from ECOS (France) and SETCIP (Argentina) through their cooperative science program (A01U04). We would also like to thank the referee for valuable comments on this paper.

REFERENCES

Abbett, W., Fisher, G. H., and Fan, Y. 2000, *Astrophys. Journ., 540,*, 548

Abbett, W., Fisher, G. H., and Fan, Y. 2001, *Astrophys. Journ., 546,*, 1194

Abramenko, V. I., Wang, T., and Yurchison, V. B. 1996, *Solar Physics., 168,* 75

Aulanier, G. and Démoulin, P. 1998, *Astron. and Astrophys., 329*, 1125

Aurass, H., Vrsnak, B., Hofmann, A., and Rudzjak, V. 1997, *Sol. Phys., 174*, 91

Berger, M. and Field, G. 1984, *Journ. Fluid Mech., 147*, 133

Berger, T. E., De Pontieu, B., Fletcher, L., Schrijver, C. J., Tarbell, T. D., and Title, A. M. 1999, *Solar Phys., 190*, 409

Biesecker *et al.* 1999, *Journ. Geophys. Res., 104, A5*, 9679

Canfield, R. C., Hudson, H. S., and McKenzie, D. E. 1999, *Geophys. Res. Lett., 26, 6,* 627

Canfield, R. C. and Reardon, K. P. 1998, *Solar Phys., 182,* 145

Chae, J., Denker, C., Spirock, T. J., Wang, H., and Goode, P. R. 2000, *Solar Phys., 195,* 333

Czaykowska, A., de Pontieu, B., Alexander, D., and Rank, G. 1999, *Astrophys. Journ., 521,* L75

Del Zanna, G., Gibson, S. E., Mason, H. E., Pike, C. D., and Mandrini, C. H. 2001 *Proceedings of 33rd COSPAR assembly, in press* 2001.

Démoulin, P., Hénoux, J. C., Priest, E. R., and Mandrini, C. H. 1996, *Astron. Astrophys., 308,* 643

Démoulin, P., Priest, E. R., and Lonie, D. P. 1996, *Journ. of Geophys. Res., 101,* 7631

Dyer, Clive, and Rodgers, David 1999, *ESA Workshop on Space Weather, ESA WPP-155*

Emonet, T. and Moreno-Insertis F. 1998, *Astrophys. Journ., 492,* 804

Fan, Y. 2001, *Astrophys. Journ., 554*, L111

Fan, Y, Zweibel, E. G., Linton, M. G., and Fisher, G. H 1999, *Astrophys. Journ., 521*, 460

Fan, Y., Zweibel, E. G., and Lantz, S. R., 1998, *Astrophys. Journ., 493*, 480

Fletcher, Lyndsay and De Pontieu, Bart 1999 *Astrophys. Journ., 520, 2*, L135

Gaizauskas, V., Mandrini, C. H., Démoulin, P., Luoni, M. L., and Rovira, M. G. 1998, *Astron. and Astrophys., 332*, 353

Galvin, A. B. and Kohl, J. 1999, *Journ. of Geophys. Res.*, 104(A5):9673–9678

Gibson S. E., and Low, B. C. 1998, *Astrophys. Journ., 493*, 460

Gibson S. E., and Low, B. C. 2000, *Journ. Geophys. Res., 105, A8*, 18187

Gibson S. E. et al. 1999, *Astrophys. Journ., 520*, 871

Gibson S. E., Mason, H. E., Pike, C. D., and Young, P. R. 1999, *Proceedings 8th SOHO Workshop, Paris, France, ESA SP-446*, 331

Gilbert, H. R., Holzer, T. E., Low, B. C., and Burkepile, J. T. 2001, *Astrophys. Journ., 549*, 1221

Glover, Alexi, Ranns, Neale D. R., Harra Louise K., and Culhane, J. Leonard 2001, *Geophys. Res. Lett., 27, 13*, 2161

Harrison et al. 1995, *Solar Phys. 162,* 233

Hudson, H. S., Lemen, J. R., St Cyr, O. C., Sterling, A. C., and Webb, D. F. 1998, *Geophys. Res. Lett, 25,* 248

Karpen, J. T., Antiochos, S. K., Hohensee, M., Klimchuk, J. A., and Macniece, P. J. 2001, *Astrophys. Journ., 553*, L85

Leka, K. D., Canfield, R. C., McClymont, A. N., and van Driel-Gesztelyi, L. 1996 *Astrophys. Journ., 462*, 547

Linton, M. G., Fisher, G. H., Dahlburg, R. B., and Fan, Y. 1999, *Astrophys. Journ., 522*, 1190

Lites, B. W. and Low, B. C. 1997, *Sol. Phys., 174*, 91

López Fuentes, M. C., Démoulin, P., Mandrini, C. H., and van-Driel-Gesztelyi, L. 2000, *Astrophys. Journ., 544*, 540

Low, B. C. 1999, In *Solar Wind Nine*, eds. S. R. Habbal, R. Esser, J. V. Hollweg, and P. A. Isenberg, AIP Conference Proceedings 471, Woodbury, New York, 109

Low, B. C. 1996, *Solar Phys., 167*, 217

Low, B. C. 1994, *Phys. of Plasmas 1*, 1684

Low, B. C. 1991, *Astrophys. Journ., 381*, 295

Mandrini, C. H., Démoulin, P., van Driel-Gesztelyi, L., Schmieder, B., Cauzzi, G., and Hofmann, A. 1996, *Solar Phys., 168*, 115

Manoharan, P. K., van Driel-Gesztelyi, L., Pick, M., and Démoulin, P. 1996, *Astrophys. Journ., 468*, L73

Martin, S. F., Bilimoria, R., and Tracados, P. W. 1994, *Solar Surface Magnetism, R. J. Rutten and C. J. Schrijver eds.* , 303

Moore, R. L., Sterling, A. C., Hudson, H. S., and Lemen, J. R. 2001, *Astrophys. Journ., 552, 2*, 833

Moore, R. L. and Roumeliotis, G. 1992 *Eruptive Solar Flares, Z. Svestka, B. V. Jackson, and M. E. Machado, eds., Lecture Notes in Physics, 399*, 69

Parker, E. N. 1987, *Astrophys. Journ., 318*, 876

Pevtsov, A. A., 2002, *Solar Phys., in press*

Pevtsov, A. A., Canfield, R. C., and Zirin, H. 1996, *Astrophys. Journ., 473*, 533

Pevtsov, A. A. and Canfield, R. C. 1999, *Magnetic Helicity in Space and Laboratory Plasmas, M.R. Brown, R.C. Canfield and A.A. Pevtsov, eds., Geophys. Monogr. Ser., AGU, Washington, D.C., vol. 111*, 103

Priest, E. R. and Démoulin, P. 1995, *J. Geophys. Res., 100,* 23443

Raadu, M. A., Schmieder, B., Mein, N., and Gesztelyi, L. 1988, *Astron. AStrophys. 197*, 289

Rust, D. M. and Kumar, A. 1994, *Sol. Phys., 155*, 69

Rust, D. M. and Kumar, A. 1996, *Astrophys. Journ., 464*, L199

Sterling, A. C., Hudson, H. S., Thompson, B. J., and Zarro, D. M. 2000, *Astrophys. Journ., 532*, 1, 628

Sterling, A. C. and Hudson, H. S. 1998, *Astrophys. Journ., 492*, L55

Spruit, H. C., Title, A. M., and van Ballegooijen, A. A. 1987, *Solar Phys., 110*, 115

Tanaka, K. 1991, *Solar Phys., 136,* 133

Tang, F. 1986, *Solar Phys., 105,* 399

Thompson, B. J., O. C. St. Cyr, S. P. Plunkett, J. B. Gurman, H. S. Hudson, R. A. Howard, and Michels, D. J. 1999, in *Sun-Earth Plasma Connections, Geophys. Monogr. Ser.,* vol. 109, edited by J. L. Burch et al., p. 31, AGU, Washington, D. C.

Titov, V. S. and Démoulin, P. 1999, *Astron. and Astrophys., 351*, 707

van Ballegooijen, A. A., and Martens, P. C. 1989, *Astrophys. Journ., 343*, 971

van Driel-Gesztelyi, Malherbe, J.-M., and Démoulin, P. 2000, *Astron. and Astrophys., 364*, 845

Wang, H., Goode, P. R., Denker, C., Yang, G., Yurchison, V., Nitta, N., Gurman, J. B., St. Cyr, C., and Kosovichev, A. G. 2001, *Astrophys. Journ., 536, 2*, 971

Zarro, D. M., Sterling, A. C., Thompson, B. J., Hudson, H. S., and Nitta, N. 1999, *Astrophys. Journ., 520, 2*, L139

Zhang, M., and Low, B. C. 2001, *Astrophys. Journ., 561, 1*, 406

This preprint was prepared with the AAS LaTeX macros v5.0.

Table 1. Timeline for disk passage of sigmoidal AR8668, from August 13 to August 26, 2001.

Days	Hours	Events
August 13		**No** relevant **CMEs** or **flares**
August 14	05:24 UT	EIT (195A) **dimming** in AR8668
	06:30 UT	LASCO-C2 (white light) **CME** in NE
	10:12 UT	EIT bright **loops** in AR8668
	11:58 UT	SXT (X-ray) sees beginning of **flare** in AR8668
	11:58-12:15 (peak 12:10) UT	GOES C7.2 **flare** in AR8668
	12:12 UT	EIT sees **flare** in AR8668
	17:52 UT	Beginnings of **cusp** in southern part of AR8668 visible to SXT
August 15	12:53-13:11 (peak 13:00) UT	GOES B7.2 **flare** in AR8668
		No relevant white light **CMEs**
August 16		Material flowing out at East limb in white light (LASCO/C2-C3) but **no CME** obviously associated with activity in AR8668
	00:18-00:48 (peak 00:34) UT	GOES C1.3 **flare** in AR8668
	08:54 UT	Meudon (H-alpha): some **filament** material in southern portion of sigmoidal filament channel
	14:00-17:00 UT	**Surges** of material in the vicinity of AR8668, visible in EIT, BBSO (H-alpha on-disk), and MLSO/PICS (H-alpha limb). Sigmoidal **filament** intermittently visible, mostly in the southern part.
	16:37-16:53 (peak 16:42) UT	GOES B8.1 **flare** in AR8668 – visible also in BBSO, **brightening** along sigmoidal filament channel
	20:23-20:35 (peak 20:29) UT	GOES C1.2 **flare** in AR8668 – visible also in BBSO, apparently localized in sunspot to the right of sigmoidal filament channel
	20:49-22:34 UT	BBSO observations show northern portion of sigmoidal **filament** apparently **erupting**, while southern part remains
August 17	03:18-03:47 (peak 03:34) UT	GOES B9.5 **flare** in AR8668
	03:24 UT	EIT **dimming** north of AR8668
	12:32-13:57 (peak 13:23) UT	GOES C2.6 **flare** in AR8668
	12:47 UT	EIT **brightening** along sigmoidal filament channel

Table 1—Continued

Days	Hours	Events
	13:13 UT	EIT **dimming** just NE of AR8668
	13:31 UT	LASCO/C2 **CME** in NE streamer
	14:12 UT	EIT NE **streamer deflection**
	14:28-17:54 (peak 16:02) UT	GOES C5.9 **flare** in AR8668
	14:34 UT	SXT **cusp** above northern portion of filament channel
	14:38 UT	EIT and BBSO **two ribbon flare** visible to NE of AR8668
	14:44 UT	BBSO and EIT **polar crown filament erupts** north of AR8668
	14:38-18:02 UT	BBSO still sees southern portion of **filament**, and northern portion becomes visible
	16:00 UT	EIT **post-flare loops** along and just NE of AR8668
	Aug 17 15:00-Aug 18 15:00 UT	MDI (photospheric magnetic field) sees **flux cancellation** near midpoint of sigmoidal filament channel
August 18		**No** relevant white light **CMEs or flares** **Filament** material visible along entire length of sigmoidal filament channel - **some motion** observed in southern portion by BBSO and **some brightening** observed in southern loops by EIT and SXT, throughout the day
August 19		Full clear sigmoidal **filament**, along entire length of sigmoidal filament channel visible throughout the day, in BBSO and Meudon. Although there is some faint material moving outwards in all directions during the day visible in LASCO C2/C3, there is no clear halo CME relatable to AR8668
	22:00 UT	**Motion** in southern part of **filament**, seen by EIT and BBSO
August 20		**No** obvious white light **CME** associated with activity

Table 1—Continued

Days	Hours	Events
		in AR8668
	06:33 UT	Full sigmoidal **filament** visible in Meudon
	07:36 UT	EIT sees **dimming** in AR8668
	08:20 UT	Southern part of **filament brightens** and **disappears** – Meudon, TRACE (171, 195, 284), EIT
	14:47 UT	EIT sees **post-flare-like loops** in AR8668
	14:59 UT	BBSO - southern part of **filament** gone (or very faint)
August 21		Beginning around 08:00 UT and throughout the day, MDI sees **emerging magnetic flux** near the midpoint of the sigmoidal filament channel
	12:30-13:30 UT	TRACE sees brightening in EFR and to the north, and motion of northern part of filament Meudon sees northern part of filament disappearing (observations end at 13:30 UT)
	14:10-14:50 UT	TRACE sees **brightening** along northern part of filament channel , and at EFR
	13:50 UT	LASCO/C2 slow **CME** in NW quadrant **No** obvious **dimming** on disk, as seen by EIT
	14:53 UT	BBSO - sigmoidal **filament mostly gone** (faint trace of southern filament remains). **Arched filament system** visible across emerging magnetic flux
	17:36-18:47 UT	**Sub-sigmoid brightening** visible in TRACE, CDS (HeI, OV, MgX, SiXII, FeXIX), EIT, and SXT
	21:00 UT	BBSO sees remaining wisp of southern **filament diappear**
August 22		No obvious **flares or CMEs** associated with AR8668 **Emerging magnetic flux** continues to grow (MDI), along with **arched filament system** (BBSO) Some **filament** material lies in southern portion of region (but difficult to tell if it is a reformation of our original filament or an independent structure Some material also visible in northern part of region (BBSO, Helio Research H-alpha) **Emerging flux region** splits the north from the south – no

Table 1—Continued

Days	Hours	Events
		longer a continuous sigmoid filament channel (BBSO)
August 23		**No** obvious **flares or CMEs** associated with AR8668
		H-alpha **filament** observations (BBSO) similar to Aug 22
August 24		**No** obvious **flares or CMEs** associated with AR8668
August 25		**No** obvious **flares or CMEs** associated with AR8668
	09:17 UT	Meudon **filament** in southern part of region visible
	14:38/54 UT	Helio/BBSO **filament** in southern part of region gone
	21:18 UT	**Jet and CME** in the vicinity of AR8668 seen in many wavelengths - LASCO, CDS, UVCS (UV), EIT, TRACE , MLSO/PICS, MLSO/CHIP (10830 Angstroms)

Note. — Multiple datasets are represented in this table: in general these do not have 24 hour coverage (although SOHO/EIT and SOHO/LASCO data did cover 24 hours and we examined these for relevant activity). Necessarily therefore not all activity during the time period is represented, but specifics for well-observed activity are given for the purpose of reference within this paper. We have erred on the side of over-inclusion, so that any activity potentially relevant to AR8668 is cited. The wavelength of observations is listed for each instrument the first time it appears in the timeline.